euspen's 21st International Conference & Exhibition, Copenhagen, DK, June 2021
www.euspen.eu

Investigations on the measurement precision of an atomic force microscope with an adjustable probe direction

Janik Schaude[1] and Tino Hausotte[1]

[1]*Institute of Manufacturing Metrology, Friedrich-Alexander University Erlangen-Nuremberg (FAU), Germany*

janik.schaude@fmt.fau.de

Abstract
The article presents measurements with an atomic force microscope (AFM) with an adjustable probe direction integrated into a nano measuring machine (NMM-1). The AFM, consisting of a commercial piezoresistive cantilever operated in closed-loop intermitted contact-mode, is based on two rotational axes, which enable the adjustment of the probe direction to cover a complete hemisphere. The axes greatly enlarge the metrology frame of the measuring system by materials with a comparatively high coefficient of thermal expansion. Therefore, the long-term measurement precision of the setup and its sensitivity to thermal variations is investigated within a thermostating housing with a long-term temperature stability of 17 mK. On the other hand, the thermostating housing necessitates long signal paths, as the signal processing units are located outside of it. Therefore, the short-term measurement precision is determined by repeated calibrations of the AFM against the traceable *z*-interferometer of the NMM-1 and the *z*-noise is determined by standstill measurements. Furthermore, the tilting-capacity of the AFM is applied for repeated measurements of a calibration grating with a nominal step height of (21.4 ±1.5) nm. It is measured while placed within the *xy*-plane of the NMM-1 and while tilted to this plane with the probe direction adjusted accordingly. The determined mean step heights for both positions of the grating with 21.42 nm and 21.18 nm and standard deviations in the double-digit pm-range agree well with the nominal step height. Furthermore, the noise-level and the short-term measurement precision are in the low single-digit nm-range. Nevertheless, the empirically determined thermal sensitivity of the sensor is about 1.3 nm/mK.

Atomic force microscopy, tilting-AFM, piezoresistive cantilever, nano measuring machine.

1. Introduction

Due to its high structural resolution, the AFM [1] was not only a prime instrument to obtain qualitative information down to the atomic-scale, but it is now also a widely used and traceable tool in nanometrology [2]. In particular the semiconductor industry's need to determine the roughness of sidewalls led to a still ongoing development of different approaches to measure (near) vertical or even undercut surface features [3]. Boot-shaped cantilever tips [4] measure critical dimensions (CD) like feature width, edge profile or line edge roughness. To improve the anisotropic stiffness of conventional CD-AFMs, a cantilever with flexure hinge structures has been shown [5]. While sidewalls are well resolved by CD-AFMs, the shape of the tip leads to a poor resolution of flat parts of a feature. Furthermore, tip characterization and the subsequent correction of the dilation caused by the finite tip size is quite laboriously, because measurements are conducted at the whole circumference of the tip [6]. Both holds true for assembled cantilevers consisting of two cantilevers glued together perpendicularly [7] or for a cantilever with an attached probing sphere [8].

A different approach to measure vertical or near vertical surface features is to introduce an inclination between the measuring object and the cantilever. This might be done by tilting the sample [9, 10], or by tilting the cantilever [11, 12, 13] in one direction. In [14] an AFM based on two rotational axes [15] to adjust the probe direction to cover a complete hemisphere has been demonstrated. While conventional AFMs are usually constructed in a very compact manner and with materials with a small thermal expansion coefficient, the two aforementioned axes greatly enlarge the metrology frame by materials with a comparatively high expansion coefficient. The AFM is therefore operated within a thermostating housing with a long-term temperature stability of 17 mK [16]. On the other hand, this thermostating housing necessitates long signal paths, as the signal processing units are located outside of it. This might make the system prone to noise. Therefore, in this paper the short-term measurement precision of the AFM is investigated in chapter 3 and its long-term measurement precision and thermal sensitivity are investigated in chapter 4. In chapter 5, repeated closed-loop scans on a calibration grating placed within the *xy*-plane of the NMM-1 and placed tilted to this plane with the probe direction adjusted accordingly are presented. The following chapter starts with the introduction of the setup, namely the mechanical design and the signal processing.

2. Setup

The flexibility to adjust the probe direction of the AFM is achieved by the utilization of a commercial SCL-Sensortech Piezo-Resistive Sensing (PRS) cantilever with a length of 110 µm, a width of 48 µm and a silicon tip with a nominal radius of <15 nm. Compared to the commonly used optical beam deflection method to measure the deflection of the cantilever, self-sensing methods, like the piezoresistive deflection measurement [17], are very compact, but still offer a high signal-to-noise ratio that is comparable to the signal-to-noise ratio of the optical beam deflection method [18]. In order to reduce contact forces and therefore to minimize elastic or plastic sample deformation, the cantilever is operated in intermitted contact-mode [19].

2.1. Mechanical design

The whole setup, shown schematically in figure 1, consists of the first axis (1), an Aerotech ANT95R-180 with a positioning range of 180° and the second axis (2), a SmarAct SR-2812 with a positioning range of 360° mounted under an angle of 45° to the first axis by an angle piece. A sensor holder (3) connects the second axis with the socket of a piezoresistive cantilever (10). The piezoelectric drive (9) stimulates the cantilever over the flexure hinge to operate the AFM in intermitted contact-mode. The whole setup is installed into a NMM-1 with a motion range of 25 x 25 x 5 mm³ and a resolution of less than 0.1 nm [20, 21]. The NMM-1 fulfils the Abbe comparator principle in all three coordinate axes by keeping the measuring system, consisting of three perpendicular interferometers (two of them are shown, namely 5 and 8) fed by stabilized He-Ne lasers, fixed and moving the measuring object (11). The measuring object is placed on a corner mirror (7) which defines the coordinate system of the NMM-1. The location of the tip of the cantilever at the intersection point of the three interferometers, the so-called Abbe point, would ensure the highest accuracy. Nevertheless, it limits the adjustment range of the probe direction to about half of a hemisphere, as the positioning range of the first axis is limited to about 90° to avoid a collision with the corner mirror. In order to sustain the full positioning range, the sensor is located 5 mm above the Abbe point. Therefore, a spacer (12) is used for flat measuring objects and invar spacers (4) enlarge the Zerodur® frame (6) of the NMM-1 to integrate the sensor system. However, the additional angle sensors and the angle control of the corner mirror about the *x*- and *y*-axis reduce the angular deviations during movement and thus any first-order deviations that arise.

The whole setup is placed within a thermostating housing and the set temperature is 20.00 °C, unless stated differently.

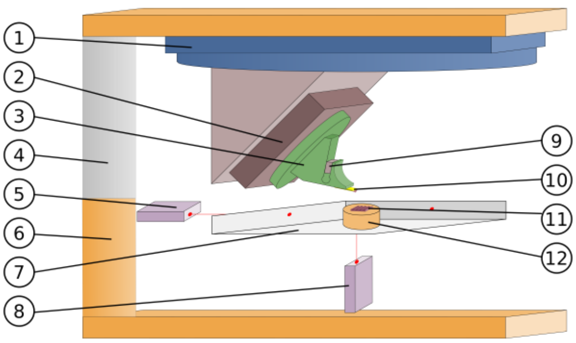

Figure 1. Simplified schematic of the setup: 1 first axis; 2 second axis; 3 sensor holder; 4 invar spacer; 5 *y*-interferometer; 6 Zerodur® frame; 7 corner mirror; 8 *z*-interferometer; 9 piezoelectric drive; 10 piezoresistive cantilever; 11 measuring object; 12 spacer.

2.2. Signal processing

The probe sensor signal evaluation is conducted with a Zurich Instruments HF2LI lock-in amplifier. A sinus signal V_{Ref} is impedance converted by a current feedback amplifier (LT1206 of Analog Devices) and stimulates the piezoelectric drive near the cantilever's resonance frequency. The signal of the piezoresistive cantilever is amplified by a commercial pre-amplifier of SCL-Sensortech. The amplified signal V_{AFM} is transduced to the lock-in amplifier, which calculates the phase-independent amplitude of the oscillation R_{AFM}. R_{AFM} is the measuring signal passed to the analog-to-digital converter of the NMM-1 with a band-limitation of 3 kHz to control the *x*-, *y*- and *z*-axis according to the probe direction specified in the measuring command. Therefore, measurements are conducted in amplitude controlled closed-loop intermitted contact-mode.

3. Short-term precision

Instead of using standards to calibrate the AFM, it was possible to use the lasers of the NMM-1. By repeating the calibration routine for several times, the short-term precision of the sensor was derived. Firstly, the second axis was in its zero position and the probe direction was against the direction of the *z*-axis of the NMM-1. Therefore, the calibration was done against the traceable *z*-interferometer. For the calibration the sample was moved towards the cantilever until full contact with a measuring velocity of 100 nm/s. The amplitude of the oscillation of the cantilever R_{AFM} and the value of the z-interferometer z_{NMM} were recorded with a point distance of 0.1 nm. The calibration was conducted 50 times within a period of time of about 2.5 minutes. For each calibration the characteristic curve $d_{AFM}(R_{AFM})$, where d_{AFM} is the deflection of the cantilever, was fitted as cubic polynomial within the intermitted contact-range. The range of the characteristic curves was therefore slightly less than the free oscillation amplitude of the cantilever.

In figure 2 the deviation $\Delta z = d_{AFM}(R_{AFM}) - z_{NMM}$ is shown, where $d_{AFM}(R_{AFM})$ is calculated by the first characteristic curve. Depicted in red are the residues of the characteristic curve, for which there is no systematic deviation perceptible. The deviations to the other 49 calibrations are shown in green.

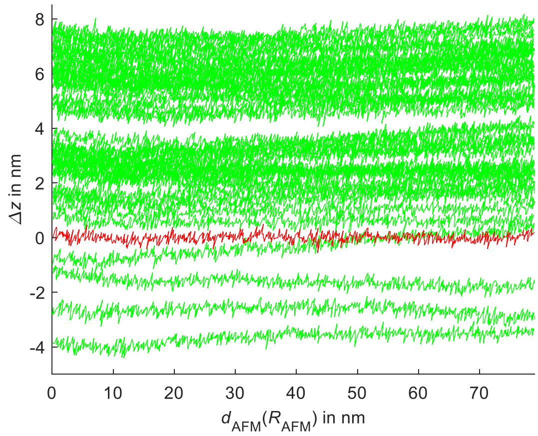

Figure 2. Deviations of the deflection of the cantilever to the *z*-values of the NMM-1 for 50 calibrations. Residues are shown in red.

To determine the short-term precision of the sensor, every characteristic curve is applied to the measuring points of every calibration and *Δz* is calculated. In figure 3, *Δz* is shown as histogram with its standard deviation $\sigma_{\Delta z}$, which is 3.8 nm. The deviations are mainly caused by variations of the offset of the characteristic curves (standard deviation 2.7 nm).

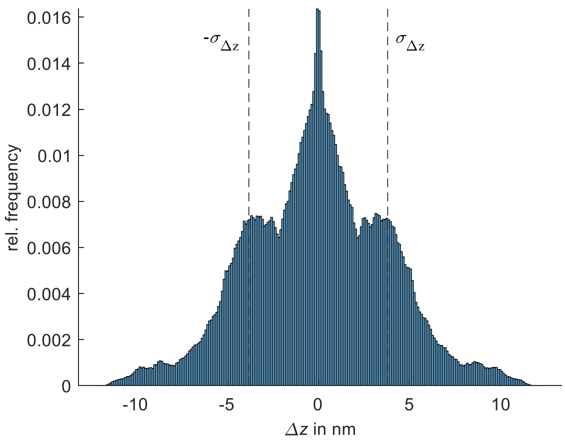

Figure 3. *Δz* as histogram with its standard deviation $\sigma_{\Delta z}$, which is 3.8 nm.

After the calibration, the controller of the NMM-1 was enabled to keep d_{AFM} in the middle of the characteristic curve and data were recorded for three times 90 s with the maximum sampling frequency of the NMM-1 (6.25 kHz). The results are shown in figure 4. The three standard deviations of z_{NMM} are 1.8 nm (red), 0.8 nm (green) and 1.3 nm (blue). The three standard deviations of d_{AFM} are 0.2 nm.

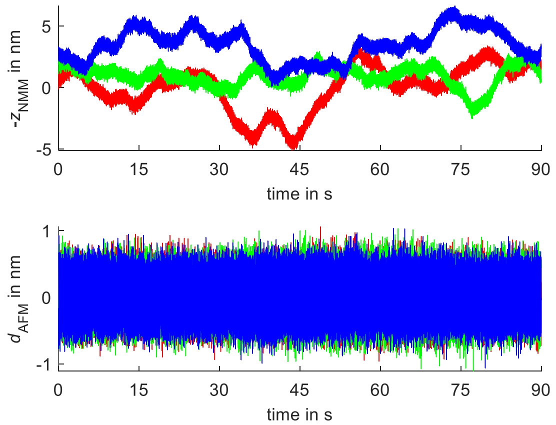

Figure 4. Three standstill measurements in closed-loop mode over 90 s.

4. Thermal sensitivity and long-term precision

To determine the thermal sensitivity and the long-term precision of the sensor, standstill measurements were conducted for 15 s every 10 minutes. The measured *z*-value z_M was calculated according to equation 1. For each measurement the offset was calculated as mean of z_M. Between the measurements the cantilever was withdrawn from the surface to avoid tip or sample damage. As tip wear occurs mainly at the beginning of a cantilever's lifetime anyway [22], this issue might be reasonably regarded as neglectable. Prior to the measurements the thermostating housing has stabilized to a temperature of 20.20 °C. Then, the set temperature was changed to 20.00 °C and the measurements have been started. The results are shown in figure 5. As can be seen, it takes about 8 hours until the offset has stabilized. Within this time the offset changes for about 260 nm, leading to a thermal sensitivity of 1.3 nm/mK. After stabilization, within the last 18 hours (shown in figure 5 below), the standard deviation of the offset is 6.7 nm.

$$z_M = -z_{NMM} + d_{AFM} \tag{1}$$

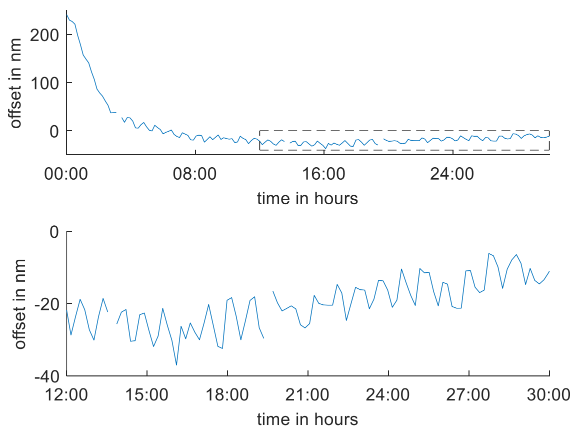

Figure 5. Variation of the offset after the set temperature was changed from 20.20 °C to 20.00 °C.

5. Scans on a calibration grating

Closed-loop scans were conducted on a calibration grating (TGZ1 of NT-MDT) with a nominal step height of (21.4 ±1.5) nm. Measured values within the (negated) coordinate system of the NMM-1 were firstly calculated according to equation 2, where $\vec{p}$ is the probe direction. As can be seen, equation 2 is a generalization of equation 1. Afterwards, the measured values were transformed into the workpiece coordinate system (WCS).

Because of the low-pass filtering associated with the calculation of d_{AFM}, as well as different analog-to-digital converters used for the probe signal and for the interferometers of the NMM-1, a latency between the signals of the interferometers and the probe signal is inevitable. In order to avoid effects caused by this latency, the scan velocity was chosen to be only 5 µm/s and the point distance was 1 nm. The scan length was 90 µm and the step height was determined according to ISO 5436-1 [23].

$$\begin{bmatrix} x_M \\ y_M \\ z_M \end{bmatrix} = -\begin{bmatrix} x_{NMM} \\ y_{NMM} \\ z_{NMM} \end{bmatrix} + \vec{p} \cdot d_{AFM} \tag{2}$$

5.1. Grating placed within the xy-plane of the NMM-1

Firstly, the grating was placed within the *xy*-plane of the NMM-1 and $\vec{p} = [0\ 0\ 1]^T$. For 30 scans the mean of the determined step heights is 21.42 nm, which agrees very well with the nominal value, and the associated standard deviation is 45 pm. The high reproducibility of the scans is also shown in figure 6, where the 30 scans of the complete scan length (above) and of an irregularity on one step (below) are depicted.

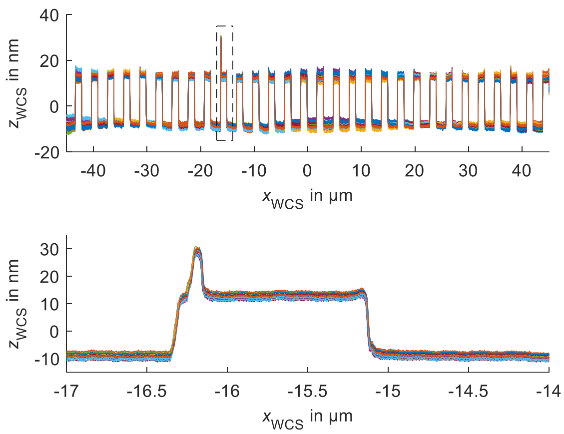

Figure 6. 30 scans of the complete scan length (above) and of an irregularity on one step (below) on the calibration grating.

5.2. Grating tilted to the xy-plane of the NMM-1

By rotating the second axis it is possible to adjust the angle between the probe direction and the *xy*-plane of the NMM-1, which is favourable if the surface normal of the measuring object is not parallel to the *z*-axis of the NMM-1. To demonstrate this, the calibration grating was placed on the NMM-1 under an angle of about 19° and the second axis was rotated accordingly ($\vec{p} = [-0.230\ 0.230\ 0.946]^T$), as is depicted in figure 7. Again, 30 scans were conducted. The mean of the determined step heights is 21.18 nm, which still agrees with the nominal value, and the associated standard deviation is 60 pm. In figure 8, the 30 scans of the complete scan length (above) and of an irregularity on one step (below) are depicted.

The slightly increased noise on the data points of the tilted grating is explainable by higher vibrations in *x*- and *y*-direction than in *z*-direction of the NMM-1. While these vibrations are completely within x_{WCS} and therefore not affecting the calculated step heights for the not tilted grating, components of these vibrations are within z_{WCS} for the tilted grating and therefore affecting the calculated step heights.

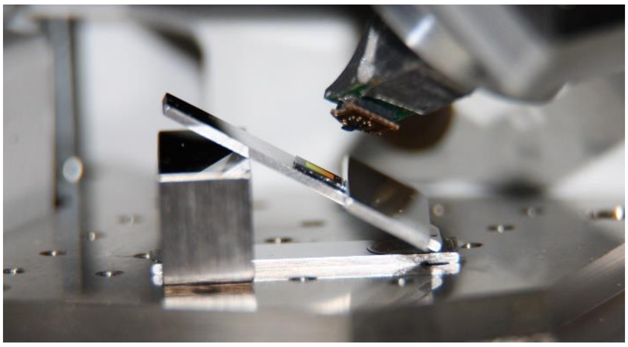

Figure 7. Calibration grating tilted to the *xy*-plane of the NMM-1 and the probe direction adjusted accordingly.

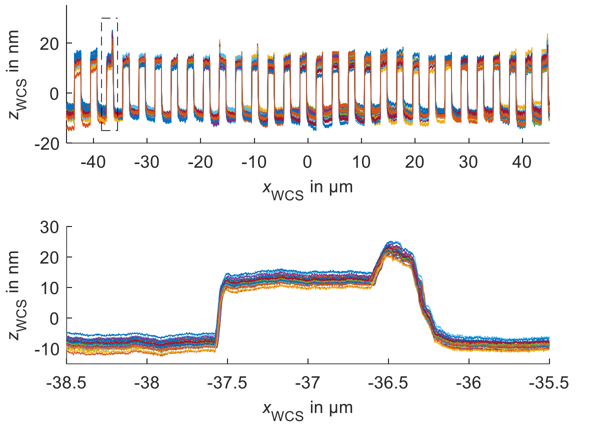

Figure 8. 30 scans of the complete scan length (above) and of an irregularity on one step (below) on the calibration grating tilted by 19° to the *xy*-plane of the NMM-1.

6. Summary, conclusion and outlook

In this article, investigations on the measurement precision of an AFM with an adjustable probe direction have been shown. The short-term precision of repeated calibrations on the NMM-1 was determined to be 3.8 nm and standstill measurements revealed standard deviations of 1.8 nm, 0.8 nm and 1.3 nm. In the long-term, the sensor has shown a precision of 6.7 nm over 18 hours and a thermal sensitivity of about 1.2 nm/mK. As a use-case of the sensor, scans on a calibration grating have been conducted, with the grating placed within the *xy*-plane of the NMM-1 and tilted to this plane with the probe direction adjusted accordingly. For both positions of the grating, the measured step height agreed well with the nominal value and the standard deviation was in the double-digit pm-range.

As has been expected, due to the integration of the rotational axes the thermal sensitivity of the sensor system is quite high. Of course, also the interferometers respond to thermal variations due to the temperature-dependent refractive index of air. For a similar interferometer, but with a dead path length of zero, a thermal sensitivity of -75 pm/mK has been reported [24]. Nevertheless, as the NMM-1 corrects the temperature-dependent variation of the refractive index of air taking the dead path length into account [25], the major portion of the determined thermal sensitivity might reasonably be attributed to the AFM and the two rotational axes. Due to the high thermal sensitivity, also the short-term measurements over only 1.5 to 2.5 minutes are affected by thermal variations. Therefore, the deviations of the repeated calibrations are mainly caused by a variation of the offsets of the characteristic curves. Nevertheless, for the standstill measurements it is possible to deduce the noise level as standard deviation of d_{AFM}, as the controller compensates the mainly temperature-induced low-frequency variations. Despite the long signal paths, the standard deviation of d_{AFM} is only 0.2 nm. As the long-term standard deviation of the temperature is about 4 mK [16], the long-term measurement precision of the sensor system with 6.7 nm is also mainly attributable to its thermal sensitivity.

Since it is probably not possible to enhance the temperature stability within the thermostating housing significantly, a reduction of the thermal sensitivity of the sensor is mandatory to enhance its measurement precision. Possible means might be the application of smaller rotational axes or a different arrangement of the axes. Placing the first axis above the Zerodur® frame (cf. figure 1), reducing the length of the invar spacers and connecting the first axis with the angle piece by materials with a low or even negative expansion-coefficient might result in compensating thermal expansions of the first axis and the remaining part of the sensor system.

Acknowledgment

This project has received funding from the EMPIR programme co-financed by the Participating States and from the European Union's Horizon 2020 research and innovation programme. The authors wish to thank for the funding.

References

[1] Binnig G, Quate C F and Gerber C 1986 *Phys. Rev. Lett.* **56** 930-933
[2] Danzebrink H-U, Pohlenz F, Dai G and Savio C D 2005 *Nanoscale Calibration Standards and Methods* **1** 3-21
[3] Yacoot A and Koenders L 2011 *Meas. Sci. Technol.* **22** 122001
[4] Martin Y and Wickramasinghe H K 1994 *Appl. Phys.* **64** 2498-2500
[5] Thiesler J, Tutsch R, Fromm K and Dai G 2020 *Meas. Sci. Technol.* **31** 074012
[6] Dahlen G, Osborn M, Liu H-C, Jain R, Foreman W and Osborne J R 2006 *Proc. SPIE* **6152** 61522R
[7] Dai G, Wolff H, Weimann T, Xu M, Pohlenz F and Danzebrink H-U 2007 *Meas. Sci. Technol.* **18** 334-341
[8] Dai G, Wolff H and Danzebrink H-U 2007 *Appl. Phys. Lett.* **91** 121912
[9] Garnaes J, Hansen P-E, Agersnap N, Davi I, Petersen J C, Kühle A, Holm J and Christensen L H 2005 *Proc. SPIE* **5878** 587803
[10] Fouchier M, Pargon E and Bardet B 2013 *Appl. Phys.* **113** 104903
[11] Hua Y, Coggins C and Park S 2010 *IEEE/SEMI ASMC* 7-10
[12] Cho S-J, Ahn B-W, Kim J, Lee J-M, Hua Y, Yoo Y K and Park S 2011 *Rev. Sci. Instrum.* **82** 023707
[13] Kizu R, Misumi I, Hirai A, Kinoshita K and Gonda S 2018 *Meas. Sci. Technol.* **29** 075005
[14] Schaude J, Albrecht J, Klöpzig U, Gröschl A C and Hausotte T 2019 *tm – Technisches Messen* **86** 12-16
[15] Schuler A, Weckenmann A and Hausotte T 2014 *Meas. Sci. Technol.* **25** 064010
[16] Gröschl A C, Schaude J and Hausotte T 2019 *tm – Technisches Messen* **86** 117-121
[17] Tortonese M, Yamada H, Barrett R C and Quate C F 1991 *TRANSDUCERS '91: 1991 International Conference on Solid-State Sensors and Actuators. Digest of Technical Papers* 448-451
[18] Dukic M, Adams J D and Fantner G E 2015 *Scientific Reports* **5** 16393
[19] Zhong Y, Inniss D, Kjoller K and Elings V B 1993 *Surface Science* **1-2** L688–L692
[20] Hausotte T, Percle B and Jäger G 2009 *Meas. Sci. Technol.* **20** 084004
[21] Hausotte T 2018 *Proc. SPIE* **10678** 106780Q
[22] Czerkas S, Dziomba T and Bosse H 2005 *Nanoscale Calibration Standards and Methods* **1** 311-320
[23] DIN EN ISO 5436-1 2000 *Beuth Verlag* Berlin
[24] Schmidt I 2008 *TU Ilmenau, dissertation*
[25] Hausotte T 2011 *Pro Business* Berlin **1**